Int. J. Heat Mass Transfer. Vol. 28, No. 10, pp. 1921–1935, 1985
Printed in Great Britain

0017–9310/85 $3.00 + 0.00

Convective flows around a rotating isothermal cylinder

BAKHTIER FAROUK and KENNETH S. BALL
Department of Mechanical Engineering and Mechanics, Drexel University, Philadelphia, PA 19104, U.S.A.

(*Received* 8 *March* 1985 *and in final form* 15 *May* 1985)

Abstract—The mixed convective flows generated by a heated horizontal cylinder rotating in air have been investigated numerically and experimentally. The presence of rotation represents an important complication and extension of previous studies on convective flow and heat transfer around heated stationary horizontal cylinders in an otherwise quiescent medium. Significant qualitative, as well as quantitative, differences in the heat transfer characteristics and flow patterns generated by the rotating cylinders are observed as compared to those for stationary cylinders. Numerical solutions are presented for wide ranges of Grashof number and the rotational parameter σ, Grashof number/(rotational Reynolds number)^2. Schlieren photographs are obtained to study the angular location of the buoyant plume for various values of the above parameter. The schlieren studies reveal that for higher rotational speeds, the flow is three-dimensional and the consequent effect on heat transfer is pronounced. Measurements of the mean Nusselt numbers are also obtained. The two-dimensional calculations predict the heat transfer characteristics satisfactorily for values of σ greater than unity.

INTRODUCTION

FREE CONVECTION heat transfer from stationary heated cylinders has been the subject of a large number of investigations. A comprehensive compilation of the experimental data can be found in [1]. Fand *et al.* [2] and Fand and Brucker [3] give an extensive survey of the work published on this subject up to 1983. Most of these studies have been restricted to a consideration of the mean heat transfer coefficient. Kuehn and Goldstein [4] and Farouk and Guceri [5] have investigated the above problem and give detailed results of the local Nusselt numbers and the velocity profiles. Churchill and Chu [6] and Kuehn and Goldstein [7] have also proposed correlations for a wide range of Rayleigh number, for both laminar and turbulent flows.

In this paper, the flows generated by and the mixed convective heat transfer from a rotating isothermal horizontal cylinder have been investigated both numerically and experimentally. The two-dimensional numerical computations have been restricted to slow rotation. Schlieren studies of the problem reveal that for higher rotational speeds, the flow becomes three-dimensional, consequently increasing the heat transfer significantly. Measurements of the mean Nusselt number are also reported for selected Grashof numbers with a wide range of the rotational Reynolds number.

The above flows are of interest in many technological applications, ranging from the cooling of rotating machinery to the design of rotating heat exchangers and heat pipes [8]. One particular application of the above problem is the drying of paper. Paper is typically dried by passing the pulp around a series of rotating cast-iron steam-heated cylinders. It is held in contact with the heated surface by means of drying felts. Usually between 30 and 70 cylinders are used, ranging in diameter from 1.2 to 1.8 m and in widths up to 10 m [9]. Cylinder speeds of 450–500 m min^{-1} are common with the surface temperature varying between 100–180°C. The performance of the paper dryer, measured by the amount of steam needed to evaporate a given amount of water or to produce a specified amount of paper, is directly related to the surface temperature [10]. Because the paper and allied products industry ranks among the top five manufacturing industries in total energy consumption, a detailed understanding of the heat transfer characteristics of rotating cylinders also has considerable economic importance [11].

BACKGROUND

Transport and flow phenomena in rotating systems have challenged engineers and scientists for a long time. Some of the classical solutions of the Navier–Stokes and conservation of energy equations were obtained for rotating systems. Heat transfer by convection to or from bodies of revolution spinning about their axes of symmetry in an otherwise undisturbed fluid has been studied analytically and experimentally by numerous authors. Comprehensive reviews are presented by Dorfman [12] and Krieth [8] for studies made prior to 1968.

Though numerous investigations have been made of free convection from horizontal stationary cylinders, the heated rotating cylinders, in spite of their wide applications, have received little attention [13–16]. Dropkin and Carmi [13] studied the above problem and came to the conclusions that when a heated cylinder is rotated in air, the heat transfer coefficient may be located in one of three distinct regions: (a) a region where its value does not change with speed of rotation; (b) a region where its value increases with

NOMENCLATURE

C_p	specific heat at constant pressure	v_r^*	radial velocity component
D	cylinder diameter	v_θ	non-dimensional angular velocity component
g	acceleration of gravity	v_θ^*	angular velocity component.
Gr	Grashof number based on cylinder diameter, $D^3\beta g(T_w - T_\infty)/\nu^2$		
k	thermal conductivity		
m	wave number of disturbance	Greek symbols	
$\overline{Nu}$	mean Nusselt number	β	thermal coefficient of volumetric expansion
$Nu(\theta)$	local Nusselt number	ε	normal total emissivity
Pr	Prandtl number, $\mu C_p/k$	λ	wavelength of disturbance
r	non-dimensional radial coordinate	θ	angular coordinate
R	cylinder radius	θ_b	breakaway (plume separation) angle
R_∞	radius of the pseudo-boundary	ν	fluid kinematic viscosity, μ/ρ
r^*	radial coordinate	ρ	density
Re	rotational Reynolds number $(R\Omega)D/\nu$	ψ	non-dimensional stream function
T	non-dimensional temperature	ψ^*	stream function
T^*	temperature	ω	non-dimensional vorticity
T_w	cylinder surface temperature	ω^*	vorticity
T_∞	reference temperature	Ω	characteristic angular velocity of the cylinder.
v_r	non-dimensional radial velocity component		

speed of rotation and is influenced by both speed and free convection; and (c) a region where its value is proportional to the speed of rotation only. Unfortunately the region (b) was not studied in detail and no information about the velocity field was given.

Etemad [14] studied the mixed convection heat transfer from a rotating horizontal cylinder and the stability of the flow around the rotating cylinder. The transition from laminar free convection (two-dimensional) flow to fully-developed secondary flows was investigated with an interferometer. It was reported that the heat transfer coefficient decreases slightly with speed for any Grashof number until it reaches a minimum at a critical rotational speed, then increases rapidly at higher rotational speeds. No effort was made, however, to establish a criterion for this critical speed as a function of the Grashof number and fluid properties. The initial decrease of $\overline{Nu}$ is explained as the effect of thickening of the thermal boundary layer. The laminar Couette flow (due to rotation) winds the hot air of the free convection plume around the cylinder and therefore increases the effective free convection thermal boundary-layer thickness.

Both Etemad [14] and Dropkin and Carmi [13] reported that the increase in heat transfer occurs for values of rotation corresponding to $\sigma\ (Gr/Re^2) = 1$. Anderson and Saunders [15] presented an analytical argument showing that a transition should occur for $\sigma = 0.8417$. Goettler [16] studied the region of slow rotation ($\sigma > 1$) by using perturbation techniques and series truncation to solve the laminar boundary-layer equations. Only two cases were investigated and agreement with interferometric studies was not conclusive.

To date, no detailed investigation of the above problem in the free convection-dominated regime has been performed. Detailed information regarding the local Nusselt number and the flow field is lacking. Numerical solutions of the problem are helpful in clarifying the flow physics and the heat transfer characteristics.

ANALYSIS

The geometry considered consists of a heated smooth horizontal cylinder rotating in an infinite Boussinesq fluid (air). To obtain the flow and temperature distributions, the Navier–Stokes, continuity and energy equations were expressed in cylindrical polar (r, θ) coordinates. The coordinate r is normal to the surface of the cylinder and is measured radially outwards from the center of the cylinder; θ is measured anticlockwise from the downward vertical axis. Using the stream function–vorticity approach, the steady-state two-dimensional laminar convection is governed by the coupled elliptic transport equations for ψ, ω and T:

$$\frac{\partial}{\partial r}\left(r\frac{\partial \psi}{\partial r}\right)+\frac{\partial}{\partial \theta}\left(\frac{1}{r}\frac{\partial \psi}{\partial \theta}\right)=-r\omega \tag{1}$$

$$\frac{\partial}{\partial r}\left(\omega\frac{\partial \psi}{\partial \theta}\right)-\frac{\partial}{\partial \theta}\left(\omega\frac{\partial \psi}{\partial r}\right)-\frac{\partial}{\partial r}\left(r\frac{\partial \omega}{\partial r}\right)-\frac{\partial}{\partial \theta}\left(\frac{1}{r}\frac{\partial \omega}{\partial \theta}\right)=Gr\left(\frac{\partial T}{\partial \theta}\cos\theta+\frac{\partial T}{\partial r}r\sin\theta\right) \tag{2}$$

and

$$\frac{\partial}{\partial r}\left(T\frac{\partial\psi}{\partial\theta}\right)-\frac{\partial}{\partial\theta}\left(T\frac{\partial\psi}{\partial r}\right)-\frac{\partial}{\partial r}\left(\frac{1}{Pr}r\frac{\partial T}{\partial r}\right)-\frac{\partial}{\partial\theta}\left(\frac{1}{Pr}\frac{1}{r}\frac{\partial T}{\partial\theta}\right)=0 \quad (3)$$

where

$$v_r=\frac{1}{r}\frac{\partial\psi}{\partial\theta},\quad v_\theta=-\frac{\partial\psi}{\partial r} \quad (4a,4b)$$

and

$$\omega=\frac{1}{r}\left\{\frac{\partial}{\partial r}(rv_\theta)-\frac{\partial v_r}{\partial\theta}\right\}. \quad (5)$$

The variables are non-dimensionalized with reference to the cylinder diameter, the kinematic viscosity and the temperature difference between the cylinder surface and the ambient:

$$r=\frac{r^*}{D},\quad T=\frac{T^*-T_\infty}{T_w-T_\infty},\quad v_r=\frac{D}{\nu}v_r^*,$$

$$v_\theta=\frac{D}{\nu}v_\theta^*,\quad \psi=\frac{\psi^*}{\mu}\quad\text{and}\quad \omega=\frac{\omega^*D^2}{\nu}. \quad (6)$$

The non-dimensional parameters Gr and Pr are defined as follows:

$$Gr=\frac{g\beta D^3(T_w-T_\infty)}{\nu^2},\quad Pr=\frac{\mu C_p}{k}.$$

Boundary conditions

For the cylinder surface $T=1$ and $\psi=0$ for $0\leqslant\theta\leqslant 2\pi$. The cylinder surface velocity is given as $v_\theta=Re$ where Re is the rotational Reynolds number $[Re=(R\Omega\cdot D)/\nu]$. An expression for the vorticity boundary condition can be obtained by expanding the stream function near the surface, using a three-term Taylor series expansion and by making use of the continuity and no-slip conditions:

$$\omega=\frac{Re}{0.5}-\frac{2\psi}{(\Delta r)^2}-\frac{2Re}{(\Delta r)} \quad (7)$$

where ψ is the value of the stream function at a distance Δr from the cylinder into the fluid.

For the far field, the necessity to limit the size of the solution domain requires that a pseudo-boundary be defined at a finite distance from the cylinder surface. Any realistic model must allow for fluid to cross the pseudo-boundary. It is assumed that the velocity component in the angular direction, v_θ, is negligible along the pseudo-boundary, implying that in the far field

$$\frac{\partial\psi}{\partial r}=\frac{\partial\omega}{\partial r}=0. \quad (8)$$

The temperature of the fluid drawn into the flow field is the same as that of the ambient fluid. However, a generalization along the entire outer boundary cannot be made since the temperature distribution along the section of the boundary where the plume crosses is not known *a priori*. It is assumed that the temperature gradient normal to the pseudo-boundary is zero implying that the heat carrying action of the fluid is primarily due to convection rather than by conduction in the far field, i.e.

$$\frac{\partial T}{\partial r}=0. \quad (9)$$

This method has been used successfully by Farouk [17].

Solution procedure

The resulting three coupled elliptic equations (for stream function, vorticity and temperature) are transformed into difference equations by using a control volume based finite-difference method [18]. A successive substitution technique is employed to solve the finite-difference equations along with the prescribed boundary conditions. The finite-difference procedure adopts an upwind difference scheme for the convective terms and a line-by-line tridiagonal matrix algorithm is employed for the solution of the discretized equations.

THE EXPERIMENTS

The test apparatus consists of an aluminum cylinder (68.58-cm long, 8.83-cm O.D.) mounted horizontally and driven by a pulley–belt system. The heating of the cylinder has been accomplished by bonding three flexible silicone rubber strip heaters to its inner surface. The cylinder surface temperature is monitored by seven thermocouples located at different axial positions and uniform (within 5%) surface temperature is obtained. A high precision slip-ring assembly is used for the transfer of the thermocouple and heater inputs from the rotating to the stationary frame. Compensating circuits have been provided to obtain accurate temperature readings of the thermocouples for a wide range of operation. The test cylinder is driven by a 90-V, 1/4-h.p. DC motor. A solid state SCR speed controller has been selected to provide constant r.p.m. operation. For lower speeds a gear reducer ensures uniformity of rotation. The drive shafts are supported by ball bearings on each side, which can resist light thrust loads. The rotational speed is measured accurately by use of a phototachometer.

The cylinder was highly polished using ordinary automobile polishes (rubbing compound and white polish). Radiation losses were calculated using a tabulated value for the emissivity of polished aluminum $\varepsilon=0.079$. To minimize end losses, transite end-caps were fabricated and attached to each end of the cylinder. Two thermocouples were placed in the end caps to estimate the lateral heat losses. Electricity is supplied to the heaters through a voltage-regulated DC source. A rheostat is used to vary power to the heater. Two digital multimeters (Fluke model 8050 A) are used to measure the voltage supplied to and the current through the heater.

For the purpose of measuring temperature from the thermocouples, a single-board computer interface (Omega Engineering, Inc. μMEGA 4000) is used. An Apple IIe microcomputer is used to operate the board and to reduce the data.

The experimental set-up is located in a laboratory which is isolated from the building's heating and ventilating systems. Adequate measures have been taken for controlled ventilation of the laboratory. The ambient fluid is checked for thermal stratification during any experimental run.

In addition to measuring mean Nusselt numbers as functions of the Grashof number and the rotational parameter σ, schlieren studies of the temperature field have also been performed. A 25.4-cm-diam. schlieren system was used along with a 100-W mercury light source. A 35-mm SLR camera (with 135-mm lens) was used to record directly the schlieren images [19]. The position and orientation of the knife-edge was adjustable in 25.4 μm increments by micrometer screws, allowing the temperature gradients to be seen normal to any radial line.

RESULTS AND DISCUSSION

The numerical solutions are presented first. Solutions were obtained for a wide range of Grashof number (1.39×10^3–1.39×10^7), with $Pr = 0.7$. For each Grashof number, the rotational parameter σ was varied from ∞ (free convection) to 1.0. The reasons for limiting the values of σ will be explained later. A 41×100 ($r \times \theta$) grid was found adequate for the computations. Both uniform and variable spacing grids were considered in the radial direction. Only a uniform grid was employed in the θ direction. For the higher Grashof number flows, denser grid spacing was used near the cylinder wall due to the sharp gradients of the dependent variables at that region. The maximum ratio of R_∞/R used in the computation was equal to 8 (for $Gr = 1.39 \times 10^3$). Smaller computational domains were considered at higher Grashof numbers. The same grid size (41×100) was hence sufficient to provide desired grid densities at high Grashof numbers. A complete check for grid independence was performed in a previous study [5].

Figures 1(a) and (b) show the isotherms and streamlines for the natural convection flow ($\sigma = \infty$) around a cylinder, the Grashof number being 1.39×10^6. At this large Grashof number, a boundary layer forms around the cylinder. The assumption of negligible curvature effects is not valid at this Grashof number, so the solution to the boundary-layer equations only does not give valid results here. The majority of the flow approaches the cylinder from the side as opposed to the bottom. Though the flow and temperature patterns were symmetric, no symmetry lines were considered and the entire cylinder surface was considered within the computational domain. Isotherm and streamline patterns at the same Grashof number but at lower values of σ are shown in Figs. 1(c)–(h). Figures 1(c) and (d) are for $\sigma = 10.0$ and the rotation of the cylinder is anti-clockwise. At this slow rotational speed, the plume shifts slightly toward the left and the streamlines undergo considerable change. The lower stagnation point disappears and the upward flow is thrown towards the left. Figures 1(e) and (f) show the isotherms and streamlines at $\sigma = 2$. The effect of buoyancy is still prominent as can be seen in the above figures. Adjacent to the rotating cylinder, the fluid is wrapped around and eventually breaks away near

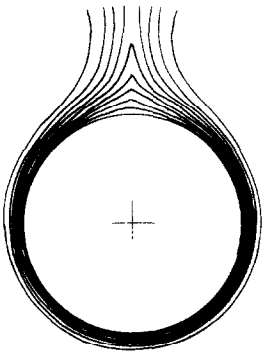

FIG. 1(a). Isotherms for $Gr = 1.39 \times 10^6$, $\sigma = Gr/Re^2 = \infty$, $\Delta T = 0.1$.

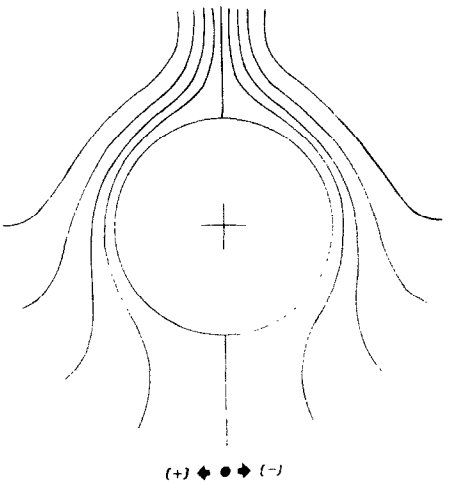

FIG. 1(b). Streamlines for $Gr = 1.39 \times 10^6$, $\sigma = \infty$, $\pm\Delta\psi = 25.70$.

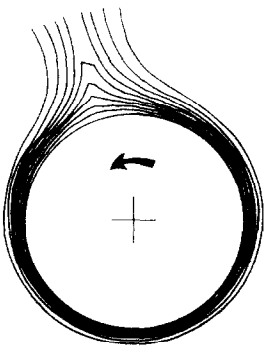

FIG. 1(c). Isotherms for $Gr = 1.39 \times 10^6$, $\sigma = 10$, $\Delta T = 0.1$.

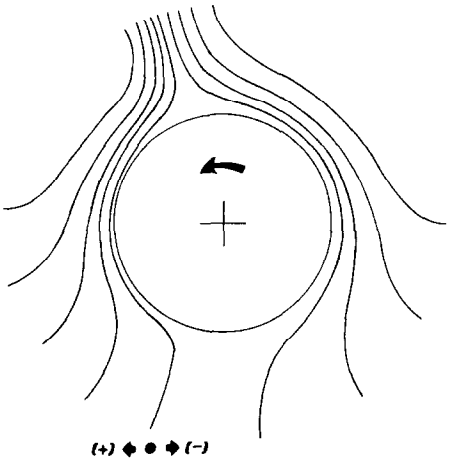

FIG. 1(d). Streamlines for $Gr = 1.39 \times 10^6$, $\sigma = 10$, $+\Delta\psi = 19.99$, $-\Delta\psi = 31.69$.

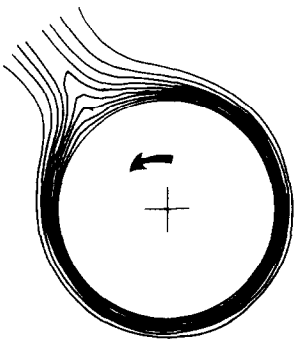

FIG. 1(e). Isotherms for $Gr = 1.39 \times 10^6$, $\sigma = 2$, $\Delta T = 0.1$.

$\theta = 210°$ and forms an upward plume. Figures 1(g) and (h) show similar results for $\sigma = 1$ where the centrifugal and buoyancy effects are of similar magnitude. The breakaway point of the thermal plume is close to $\theta = 270°$. Due to the high rotational Reynolds number, the near field is strongly dominated by the centrifugal effects. However, buoyancy effects dominate away from the cylinder, where an upward plume forms and the flow field becomes distorted.

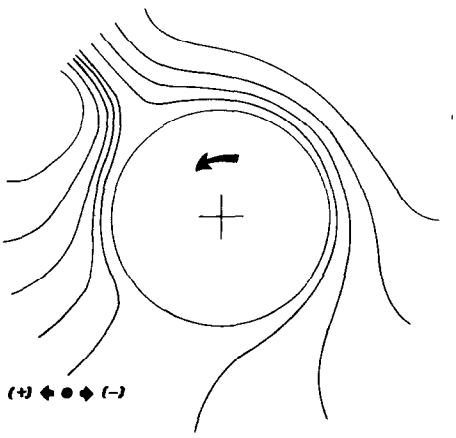

FIG. 1(f). Streamlines for $Gr = 1.39 \times 10^6$, $\sigma = 2$, $+\Delta\psi = 13.34$, $-\Delta\psi = 38.86$.

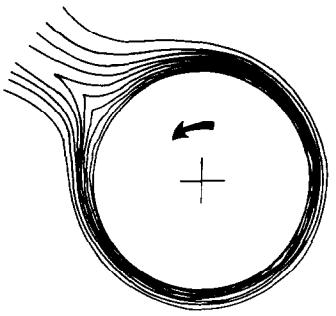

FIG. 1(g). Isotherms for $Gr = 1.39 \times 10^6$, $\sigma = 1$, $\Delta T = 0.1$.

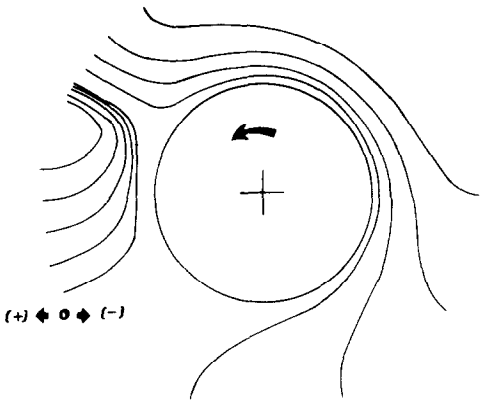

FIG. 1(h). Streamlines for $Gr = 1.39 \times 10^6$, $\sigma = 1$, $+\Delta\psi = 7.87$, $-\Delta\psi = 44.11$.

Figure 2(a) shows the mean Nusselt number as a function of the reciprocal of σ for various Grashof numbers. Some experimental measurements are also shown in the above figure. It is generally seen that the computed mean Nusselt number decreases gradually with increasing rotational speed for any given Grashof number. Neglecting free convection, the flow due to an infinitely long isolated cylinder rotating about its axis in a viscous fluid consists of concentric circular streamlines, the velocity being inversely proportional to the radius. For a heated cylinder the corresponding steady heat transfer between fixed temperatures at the cylinder surface and in the field at infinity, due to thermal conduction alone, is theoretically zero [15]. In this regard, our two-dimensional calculations give consistent results. However, this flow is known to become unstable at a specific speed of rotation, depending on the Grashof number. For zero Grashof number, the Reynolds number where instability sets in is between 35 and 50 [20]. Our experiments, as well as those of Etemad [14], show that for the mixed convective flow problem the instabilities set in near $\sigma = 1$ and the flow becomes three-dimensional. The numerical results are thus restricted to the lower value of $\sigma = 1$ for any given Grashof number.

The experimental values shown in Fig. 2(a) show almost uniform mean Nusselt numbers for $1/\sigma$ varying from 0 to 1. Nusselt number values do not show any dip near $\sigma = 1$ and the reason is explained later when the schlieren study results are discussed. The mean Nusselt

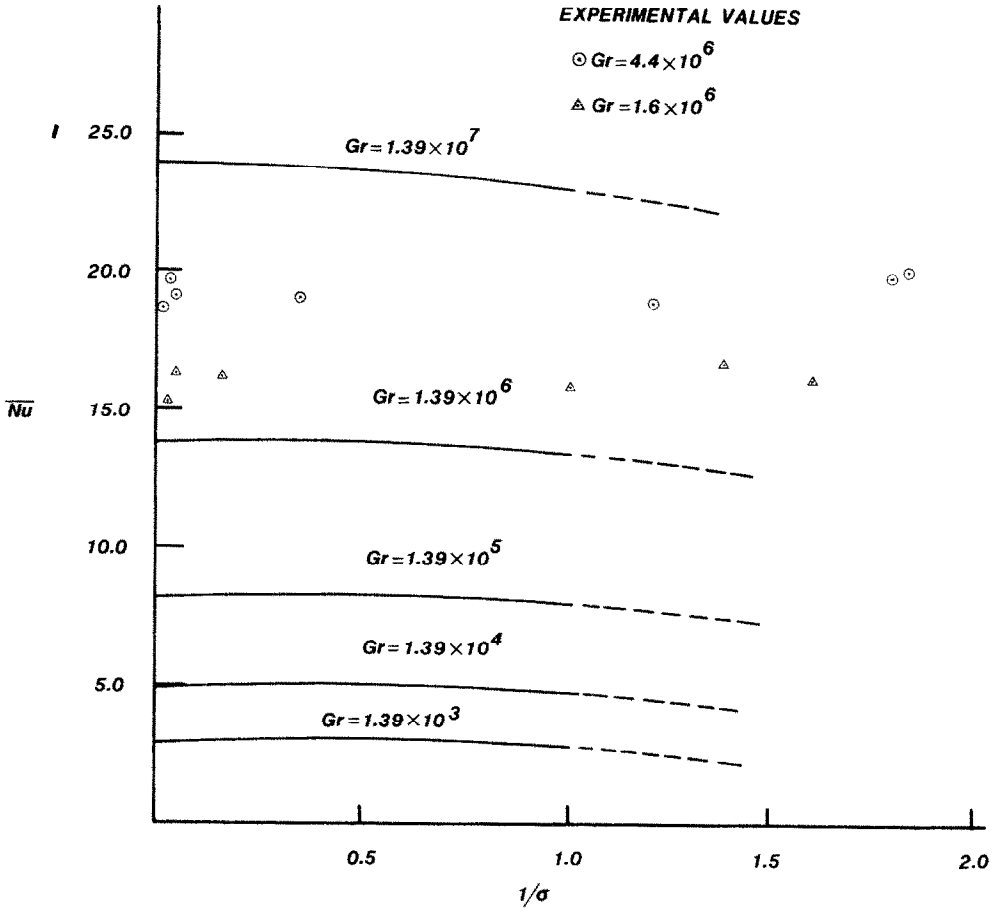

FIG. 2(a). Mean Nusselt number as a function of σ (Gr/Re^2) for various Grashof numbers.

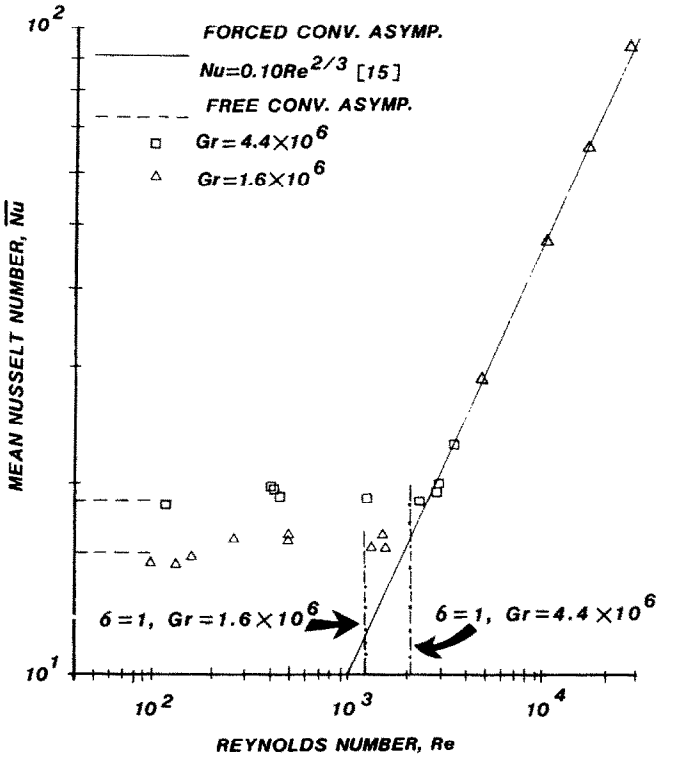

FIG. 2(b). Mean Nusselt number as a function of Reynolds number for selected Grashof numbers.

number values for higher Reynolds number cases could not be shown in Fig. 2(a) because of the limited scale. These are shown in Fig. 2(b).

Figure 2(b) shows the variation of $\overline{Nu}$ as a function of Reynolds number for selected Grashof numbers. Only the experimental measurements are included in this figure. As shown in the earlier figure, the mean Nusselt number remains fairly constant and then increases rapidly for large values of Reynolds number (lower values of σ) and ultimately the heat transfer results become independent of the Grashof number. The forced convection and free convection asymptotes (for the two Grashof numbers) are also included in the figure. The $\sigma = 1$ locations on the abscissa for the two Grashof numbers considered are also shown in Fig. 2(b) to provide continuity with Fig. 2(a).

Figure 3 gives the local Nusselt number predictions for the mixed convective flows where $Gr = 1.39 \times 10^6$. At $\sigma = \infty$ the local Nusselt number distribution is symmetric and the predictions agree well with a previous study by Kuehn and Goldstein [4]. Though the mean Nusselt number undergoes minor changes with variation of σ, the local distribution varies significantly with changing σ. Due to the anti-clockwise rotation of the cylinder, the minimum local Nusselt number shifts towards increasing θ and the 'minimum point' gradually increases in value. On the ascending side of the cylinder the local Nusselt number variation is gradual whereas it changes more rapidly on the descending side.

Computed angular velocity distributions at $Gr = 1.39 \times 10^6$ are shown in Figs. 4(a) and (b) at $\theta = 90°$ and $\theta = 270°$, respectively, for various values of σ. At $\theta = 90°$, the rotation aids the upward flow near the wall due to buoyancy. The peak of the angular velocity progressively moves nearer to the wall with higher speeds of rotation and in the far field, the velocity profiles for the mixed convection cases follow the free convection ($\sigma = \infty$) profile. As shown in Fig. 4(b), rotation opposes the upward flow at $\theta = 270°$. Large gradients of the angular velocity profiles are present near the cylinder wall at higher rotational speeds and the velocity profile flattens out faster at the far field for small values of σ. It is interesting to note that the local Nusselt number decreases at $\theta = 90°$ for increasing rotational Reynolds number and increases at $\theta = 270°$ for the same effect (Fig. 3).

Computed radial velocity distributions at $\theta = 90°$ and $\theta = 270°$ for $Gr = 1.39 \times 10^6$ are shown in Figs. 5(a) and (b) for various values of rotation parameter σ. At $\theta = 90°$, the radial velocity is inward for all values of σ. It is observed that for the pure natural convection case, the radial velocity magnitude at the far field is significant, indicating that a major portion of the incoming flow is coming from the sides. As the rotational Reynolds number increases, the magnitude of the radial velocity is amplified uniformly along the radial line. At $\theta = 90°$, both the rotational and centrifugal effects aid the flow and the effects are evident in Figs. 4(a) and 5(a). Quite opposite effects are observed in Fig. 5(b) where the radial velocity distributions are shown at $\theta = 270°$. For higher rotational speeds, an outward flow is observed

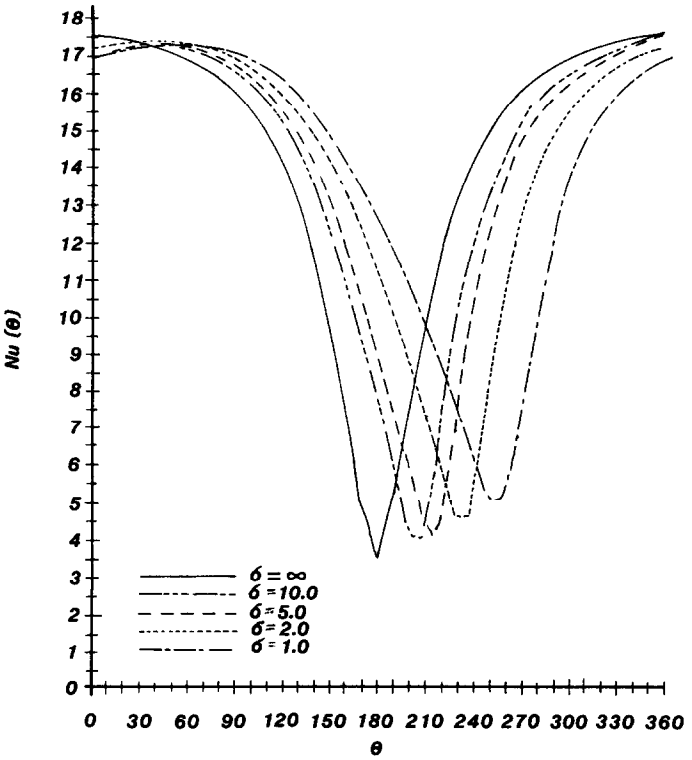

FIG. 3. Local Nusselt number distributions for various values of σ, $Gr = 1.39 \times 10^6$.

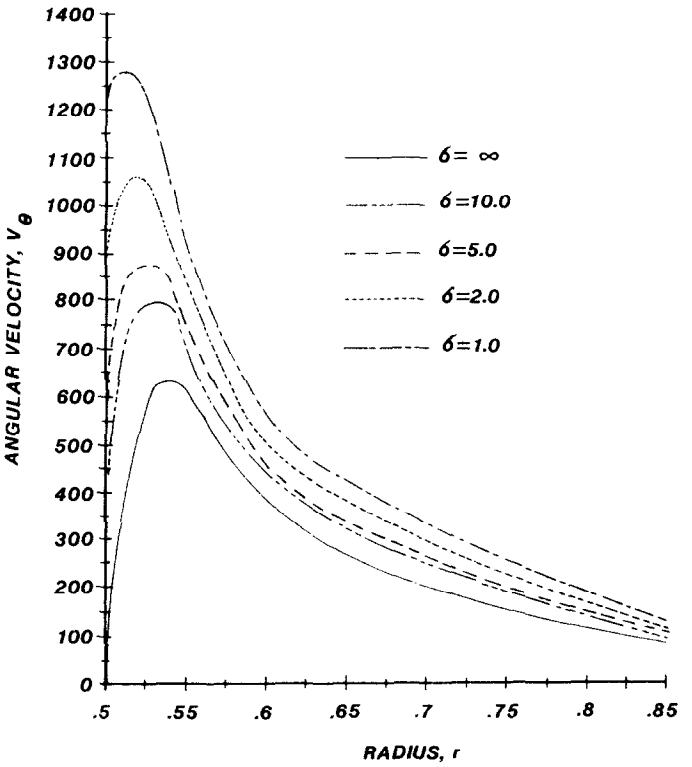

FIG. 4(a). Angular velocity distributions at $\theta = 90°$, $Gr = 1.39 \times 10^6$ for various values of σ.

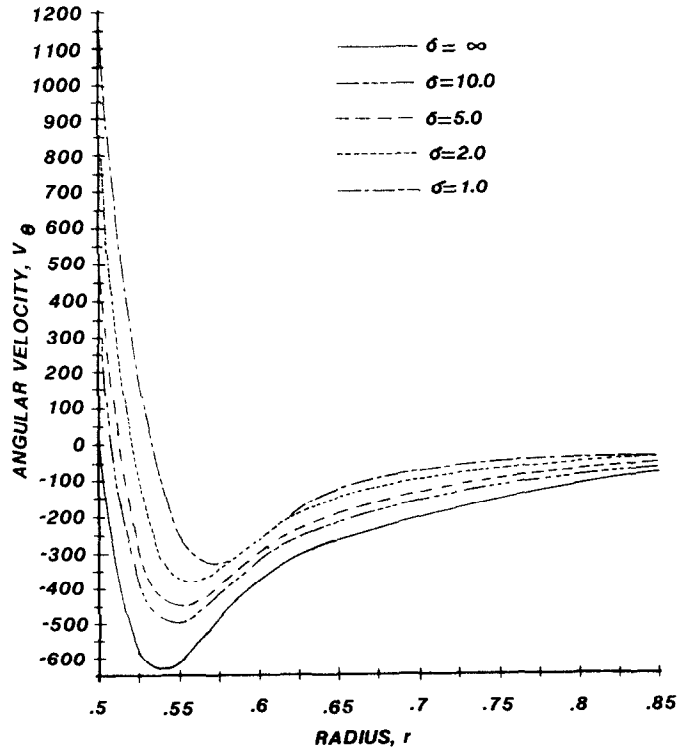

FIG. 4(b). Angular velocity distributions at $\theta = 270°$, $Gr = 1.39 \times 10^6$ for various values of σ.

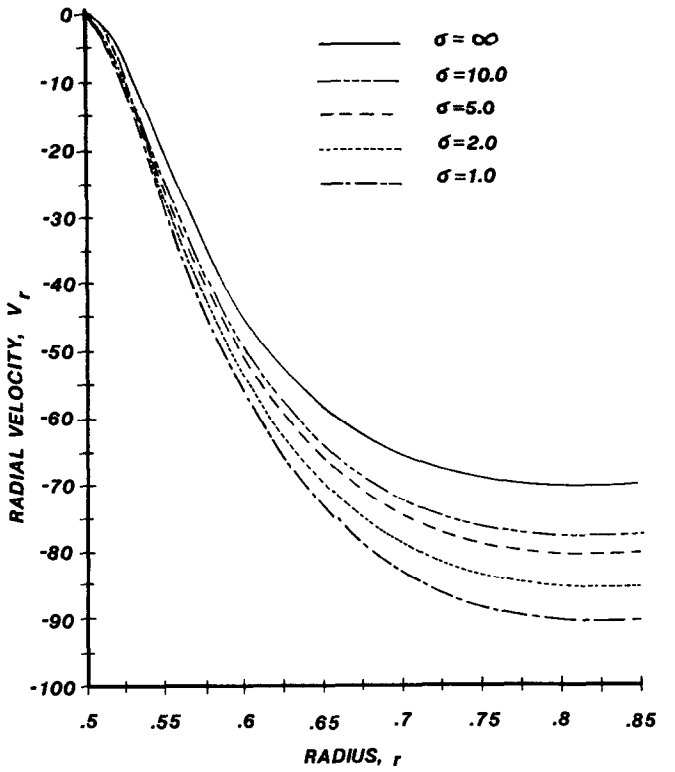

FIG. 5(a). Radial velocity distributions at $\theta = 90°$, $Gr = 1.39 \times 10^6$ for various values of σ.

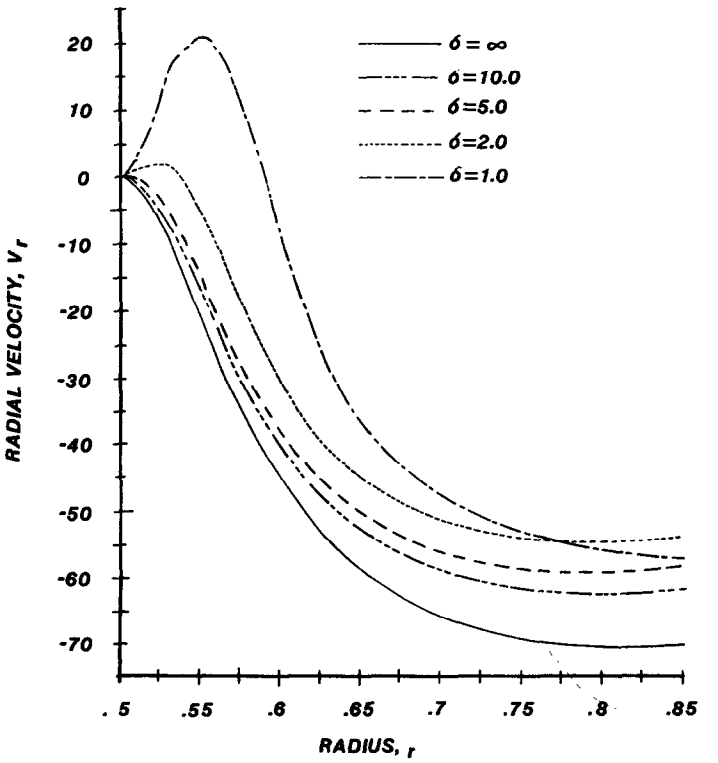

FIG. 5(b). Radial velocity distributions at $\theta = 270°$, $Gr = 1.39 \times 10^6$ for various values of σ.

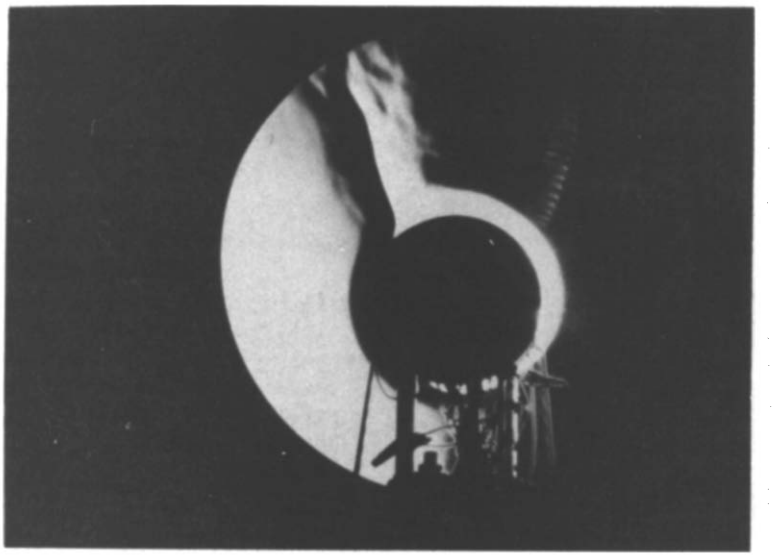

FIG. 6(a). Schlieren photograph of plume location, $Gr = 4.635 \times 10^6$, $\sigma = \infty$.

near the cylinder and the velocity profile drops off at a faster rate in the far field.

Schlieren photographs of the temperature field for values of rotational speed corresponding to $\sigma = \infty$, 3.333 and 0.6349 are shown in Figs. 6(a)–(c), respectively. The Grashof number for these photographs is 4.6×10^6. Similar behavior was noted for all Grashof numbers studied.

In Fig. 6(a), the extent of the thermal boundary layer can be seen along with the plume location (at the top), and the fact that the flow appears to be laminar. Figures 6(b) and (c) show the progressive shift of the plume in the direction of rotation (anti-clockwise). The beginning of turbulence in the outer region of the plume can be seen in Fig. 6(b), but the flow in the area of the cylinder surface remains laminar. In Fig. 6(c), substantial amounts of hotter fluid can be seen around the outer edge of the thermal boundary layer. This fluid, which is thrown radially outward, appears as wisp-like threads near the top of the cylinder and the location of the plume. This behavior rapidly becomes pronounced and accompanies the total breakdown of the plume as σ is decreased in value below unity.

Figures 7(a)–(c) show the transition of the flow from a laminar, two-dimensional flow to a three-dimensional, yet still largely laminar, secondary mean flow. These pictures were all taken in the transverse direction to show variations of temperature gradient in the axial direction, and the Grashof number was 4.4×10^6.

Figure 7(a) is for the case where $\sigma = \infty$ (free

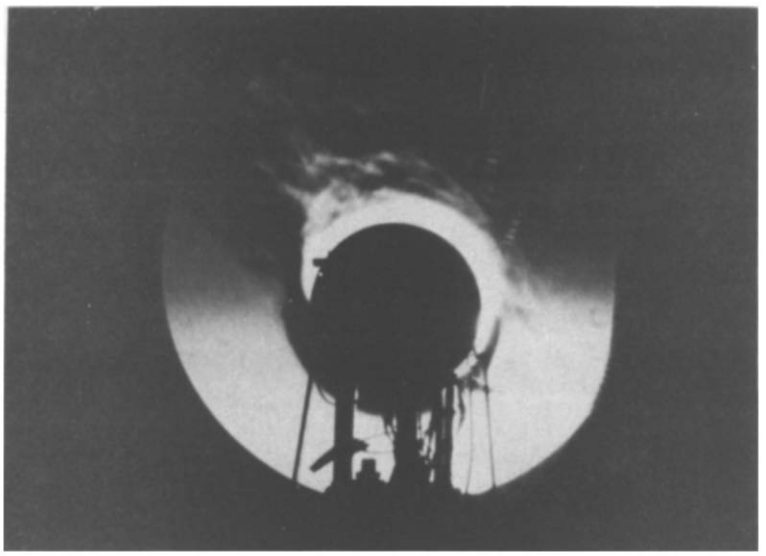

FIG. 6(b). Schlieren photograph of plume location, $Gr = 4.818 \times 10^6$, $\sigma = 3.333$.

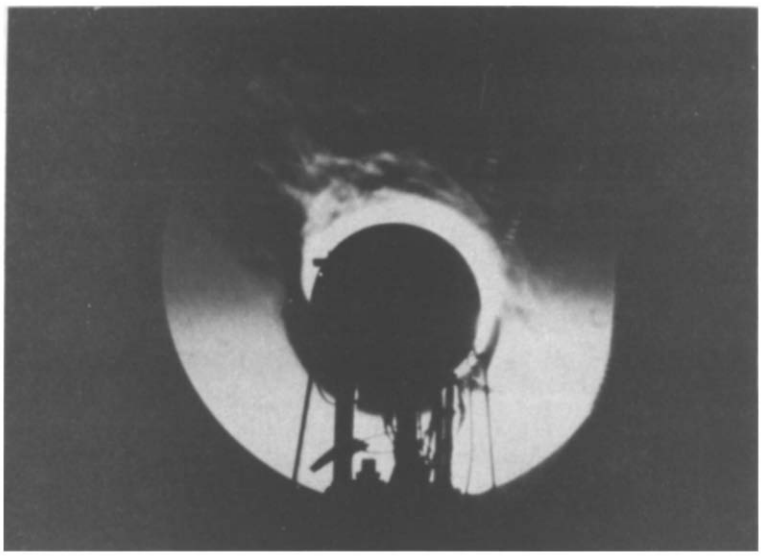

FIG. 6(c). Schlieren photograph of plume location, $Gr = 4.762 \times 10^6$, $\sigma = 0.6349$.

convection). The thermal boundary layer is seen to be two-dimensional and laminar. As rotation is increased, some periodic disturbances are seen in the boundary layer, but the overall flow structure is predominately unaffected and remains two-dimensional and laminar. Such a disturbance is seen in Fig. 7(b), where $\sigma = 1.350$. The frequency of these disturbances increases as σ is decreased, until a critical value of σ is reached below which the flow is permanently altered. The transition to this three-dimensional secondary flow is gradual, occurring over the range of σ from unity to approx. $\sigma = 0.5$. The structure of this new flow regime can be seen in Fig. 7(c), where $\sigma = 0.1168$.

Some general observations can be made about this flow. First, the upper half of the cylinder appears to become unstable and undergo total transition prior to the bottom half. Secondly, the secondary flow appears to be stable and stationary over the range of σ from transition down to $\sigma \approx 0.01$, at which time the flow structure appears to break down and become totally turbulent. Third, the flow appears to have a periodic form in the axial direction, with a fixed wave number that does not change with increasing speed of rotation. The wave number m $(=2\pi/\lambda)$ was measured as $m = 4.476 \pm 15\%$ cm^{-1}.

Finally, the critical values of σ for which the flow is seen to undergo transition in the schlieren photographs corresponds to a marked increase in the heat transfer rates. It thus appears that this increase in mean Nusselt number is due to a stable, laminar secondary mean

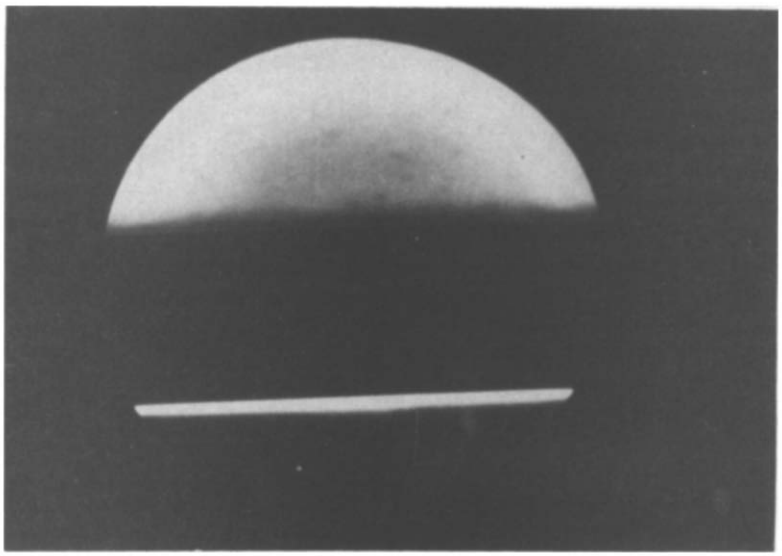

FIG. 7(a). Schlieren photograph showing axial disturbances of temperature field, $Gr = 4.57 \times 10^6$, $\sigma = \infty$.

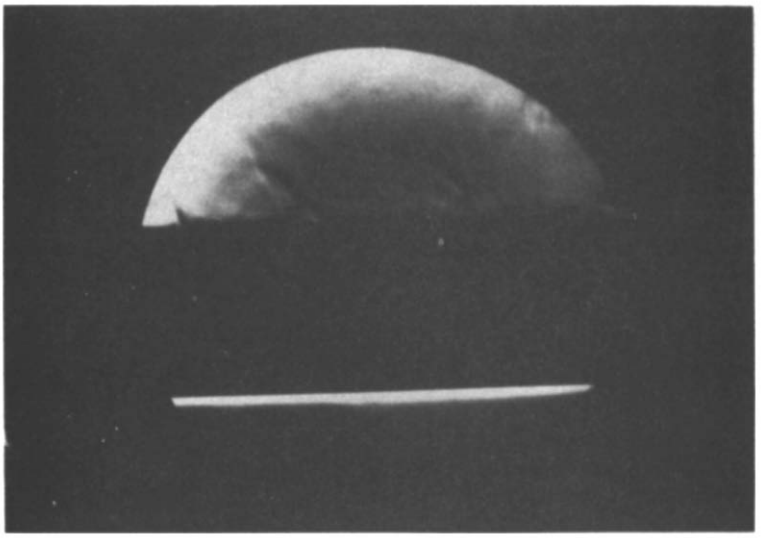

FIG. 7(b). Schlieren photograph showing axial disturbances of temperature field, $Gr = 4.482 \times 10^6, \sigma = 1.350$.

flow, and not due to the onset of turbulence as previously suggested. Disturbances in the axial direction which exist prior to transition may account for the absence of a dip in the mean Nusselt number measurements near $\sigma = 1$. The periodic nature of this flow suggests a form similar to the Taylor-vortex instability, and the mechanisms causing this transition and the onset of Taylor vortices in an annulus are most likely closely related.

The shifting of the plume due to increasing rotational speed is shown in Fig. 8. The angular location of the centerline of the plume at $r^* = R$, the breakaway angle θ_b, is measured from the top of the cylinder and is positive in the direction of rotation (anti-clockwise). For low rotational speeds, the position of the plume is expected to be directly proportional to the speed, or inversely proportional to the square root of σ. This has been verified by Shimomura [21], who proposed the relation $\theta_b = 84.9\,(Re/\sqrt{Gr})$. Excellent agreement with Shimomura was obtained in both the schlieren and the numerical studies up to a value of $\sigma = 2.77$ $(Re/\sqrt{Gr} = 0.6)$. Below this value of σ, both sets of data deviate from Shimomura's. In this region, the value of θ_b is inversely proportional to σ. This result verifies the importance of σ as the rotational parameter of interest; as σ nears unity, the centrifugal to buoyancy force ratio becomes the important predictive parameter.

In the schlieren photographs of Fig. 6, the centerline of the plume is seen as the divider between the light and dark regions of the plume. The angular orientation of the knife edge was changed for each value of σ so that

FIG. 7(c). Schlieren photograph showing axial disturbances of temperature field, $Gr = 4.351 \times 10^6, \sigma = 0.1168$.

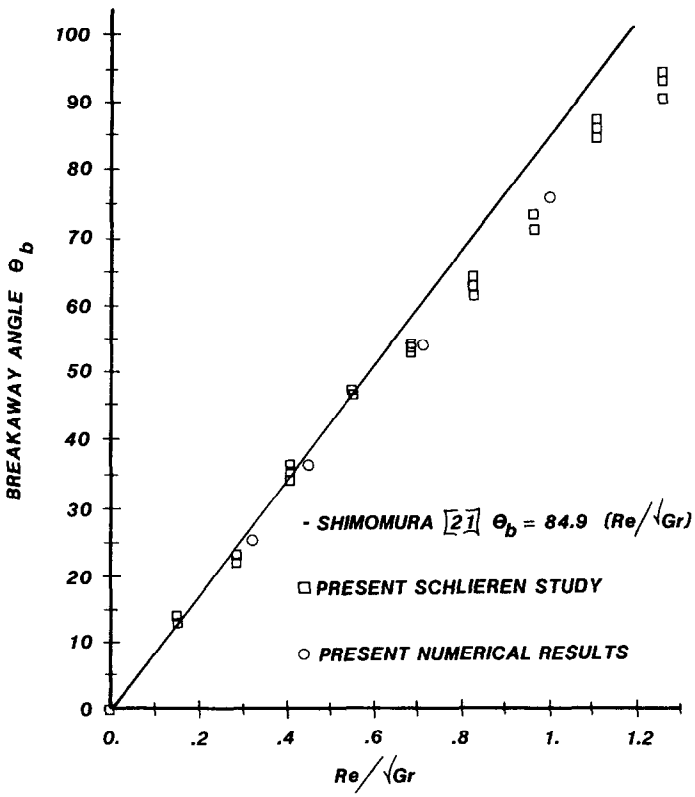

FIG. 8. Plume breakaway position as a function of the rotational parameter σ.

the intersection of the centerline with the cylinder surface was plainly visible. This method of locating the breakaway angle of the plume is more accurate than the 'grid' type of schlieren photograph obtained by Shimomura [21], and is probably the reason for the discrepancy in data.

The physical importance of the plume breakaway angle is that this location corresponds to the minimum local Nusselt number. Furthermore, as σ nears the critical value for transition to the secondary flow regime (and increased heat transfer rates), the plume position begins to oscillate and eventually the plume breaks down. Thus, the behavior of the plume has a significant influence on the overall problem.

CONCLUSION

A detailed investigation of the convective flows around a rotating isothermal cylinder has been completed. Numerical computations were carried out for the free convection dominated flow regime. Experimental studies show that this regime is two-dimensional in nature, with the mean heat transfer rates remaining essentially constant. As the rotational speed of the cylinder is increased, three-dimensional disturbances in the form of axial waves appear, with transition to a secondary, three-dimensional mean flow finally occurring at values of the rotational parameter σ just slightly lower than unity (where forced convection effects begin to dominate). The mean heat transfer rates undergo a marked increase with rotational speed in the three-dimensional regime.

Numerical studies of the two-dimensional problem have revealed detailed qualitative, as well as quantitative information about the flow field and the local heat transfer rates that was previously lacking in the literature. One significant result is the prediction of the angular location of the minimum local Nusselt number $Nu(\theta)$, which corresponds to the thermal plume breakaway angle θ_b. Excellent agreement between the numerical predictions of θ_b and the breakaway angles measured from the schlieren photographs was obtained, thereby lending confidence to the validity of the numerical solutions.

Because a two-dimensional formulation was used, numerical solutions were necessarily restricted to values of σ from unity and above. The experimental study clearly shows the onset of a three-dimensional secondary flow, and the consequent increase in the heat transfer rates. It is noted that the secondary mean flow is similar in nature to the Taylor-vortex flow in an annulus, and occurs in the region of σ where the centrifugal forces begin to dominate the buoyancy force. Evidence of this is seen in the schlieren photographs, where streaks of hot fluid are first seen to be thrown away radially from the cylinder surface. Further experimental work, including local measurements of the velocity and temperature profiles, as well as extensions to the numerical formulation to include the three-dimensionality of the flow, are currently being undertaken by the investigators.

Acknowledgements—The authors gratefully acknowledge support from NSF grant MEA-83075606. They also express gratitude for the helpful suggestions made by Professor Richard Goldstein for obtaining the schlieren photographs.

REFERENCES

1. V. T. Morgan, The overall convective heat transfer from smooth circular cylinders. In *Advances in Heat Transfer*, Vol. 11. Academic Press, New York (1977).
2. R. M. Fand, E. W. Morris and M. Lum, Natural convection heat transfer from horizontal cylinders to air, water and silicone oils for Rayleigh numbers between $3 \times 10^*$ and $2 \times 10^*$, *Int. J. Heat Mass Transfer* **20**, 1173–1184 (1977).
3. R. M. Fand and J. Brucker, A correlation for heat transfer by natural convection from horizontal cylinders that accounts for viscous dissipation, *Int. J. Heat Mass Transfer* **26**, 709–726 (1983).
4. T. H. Kuehn and R. J. Goldstein, Numerical solution to the Navier–Stokes equations for laminar natural convection about a horizontal isothermal circular cylinder, *Int. J. Heat Mass Transfer* **23**, 971–979 (1980).
5. B. Farouk and S. I. Guceri, Natural convection from a horizontal circular cylinder—laminar regime, *J. Heat Transfer* **103**, 522–527 (1981).
6. S. W. Churchill and H. H. S. Chu, Correlating equations for laminar and turbulent free convection from a horizontal cylinder, *Int. J. Heat Mass Transfer* **18**, 1049–1053 (1975).
7. T. H. Kuehn and R. J. Goldstein, Correlating equations for natural convection heat transfer between horizontal circular cylinders, *Int. J. Heat Mass Transfer* **19**, 1127–1134 (1976).
8. F. Kreith, Convection heat transfer in rotating systems. In *Advances in Heat Transfer*, Vol. 5. Academic Press, New York (1968).
9. G. L. Wedel, Performance of dryer siphons, *TAPPI* **66**, No. 7, 90–93 (1983).
10. R. D. Perrault, Troubleshooting the dryer section, *TAPPI* **66**, No. 9, 65–68 (1983).
11. J. M. Duke, Federal programs for energy conservation in the paper industry, TAPPI Conference Paper 9-1, Atlanta (1977).
12. L. A. Dorfman, *Hydrodynamic Resistance and the Heat Loss of Rotating Solids*. Oliver & Boyd, Edinburgh (1963).
13. D. Dropkin and A. Carmi, Natural convection heat transfer from a horizontal cylinder rotating in air. *Trans. Am. Soc. mech. Engrs* **79**, 741–749 (1957).
14. G. A. Etemad, Free convection heat transfer from a rotating horizontal cylinder to ambient air with interferometric study of flow, *Trans. Am. Soc. mech. Engrs* **77**, 1284–1289 (1955).
15. J. T. Anderson and O. A. Saunders, Convection from an isolated heated horizontal cylinder rotating about its axis, *Proc. R. Soc.* **A217**, 555–562 (1953).
16. L. L. Goettler, Free convection from a slowly rotating horizontal cylinder. Ph.D. dissertation, University of Massachusetts (1974).
17. B. Farouk, Mixed convective flows around a slowly rotating isothermal sphere, *J. Heat Transfer* **107**, 431–438 (1985).
18. A. D. Gosman, W. M. Pun, A. K. Runchal, D. B. Spalding and M. Wolfshtein, *Heat and Mass Transfer in Recirculating Flows*. Academic Press, New York (1969).
19. R. J. Goldstein, *Optical Measurements of Temperature, Measurement Techniques in Heat Transfer* (Edited by E. R. G. Eckert and R. J. Goldstein). Technivision Services, Slough, U.K. (1970).
20. E. G. Richardson, The circulation due to a cylinder rotating in a viscous fluid, *Phil. Mag.* **1**, 1215 (1931).
21. R. Shimomura, Free-convection heat transfer from a horizontal cylinder rotating in air by the schlieren method. *Trans. Japan Soc. mech. Engrs* **29**, 1352–1359 (1963).

ECOULEMENTS CONVECTIFS AUTOUR D'UN CYLINDRE ISOTHERME ET TOURNANT

Résumé—Les écoulements convectifs mixtes créés par un cylindre horizontal chaud et tournant dans l'air ont été étudiés numériquement et expérimentalement. La présence de la rotation présente une importante complication et une expérience des études antérieures sur l'écoulement convectif et le transfert thermique autour d'un cylindre horizontal chaud et stationnaire dans un milieu au repos. Des différences qualitatives aussi bien que quantitatives dans le transfert et la configuration d'écoulement sont observées en comparaison avec les cylindres immobiles. Des solutions numériques sont présentées pour des larges domaines de nombre de Grashof, de paramètre rotationnel τ et de nombre de Grashof/(nombre de Reynolds rotationnel)^2. Des photographies schlieren sont obtenues pour étudier la position angulaire du panache pour différentes valeurs des paramètres précédents. Les études schlieren révèlent que pour les vitesses de rotation élevées l'écoulement est tridimensionnel et que l'effet sur le transfert thermique est prononcé. Des mesures des nombres de Nusselt moyens sont aussi obtenues. Des calculs bidimensionnels prédisent de façon satisfaisante les caractéristiques de transfert thermique pour des valeurs de τ supérieures à l'unité.

KONVEKTIONSSTRÖMUNGEN AN EINEM ROTIERENDEN ISOTHERMEN ZYLINDER

Zusammenfassung—Die durch einen beheizten, in Luft rotierenden horizontalen Zylinder erzeugten Mischkonvektionsströmungen sind numerisch und experimentell untersucht worden. Die Berücksichtigung der Zylinderrotation stellt eine wichtige Erweiterung früherer Untersuchungen dar, die sich mit Konvektionsströmungen und Wärmeübergang um beheizte, nicht rotierende, horizontale Zylinder in einem ebenfalls ruhenden Medium befassen. Es werden sowohl qualitative als auch quantitative Unterschiede zwischen dem rotierenden und dem ruhenden Zylinder bezüglich des Wärmeüberganges und der Strömungsformen festgestellt. Für einen großen Bereich der Grashof-Zahl und des Rotationsparameters σ, Grashof-Zahl/Reynolds-Zahl bei Rotation, werden numerische Lösungen angegeben. Um den Winkel der Auftriebsfahne bei unterschiedlichen Werten der obengenannten Parameter zu untersuchen, wird die Methode der Schlieren-Photographie angewandt. Aus den Schlierenuntersuchungen geht hervor, daß bei größeren Rotationsgeschwindigkeiten dreidimensionale Strömungsverhältnisse vorliegen. Die Auswirkungen auf den Wärmeübergang werden diskutiert. Außerdem werden Messungen der mittleren Nusselt-Zahl durchgeführt. Für Werte von σ größer als Eins erlauben die zweidimensionalen Berechnungen eine zufriedenstellende Vorhersage des Wärmeübertragungsverhaltens.

КОНВЕКТИВНЫЕ ТЕЧЕНИЯ У ВРАЩАЮЩЕГОСЯ ИЗОТЕРМИЧЕСКОГО ЦИЛИНДРА

Аннотация—Численно и экспериментально изучаются смешанноконвективные течения, возникающие у вращающегося в воздушной среде горизонтального цилиндра. Наличие вращения является серьезным усложнением и обобщением ранее проведенных исследований по конвективным течениям и теплопереносу около нагреваемых неподвижных горизонтальных цилиндров в покоящейся среде. Наблюдаются существенное качественное и количественное отличия характеристик теплопереноса и режимов течения, возникающих в результате вращения цилиндров, по сравнению с характеристиками неподвижных цилиндров. Численные решения представлены для широких диапазонов числа Грасгофа и параметров вращения σ [число Грасгофа/(вращательное число Рейнольдса)^2]. Получены шлирен-фотографии для изучения углового положения всплывающего потока для различных значений обоих параметров. Исследования, проведенные шлирен-методом, показывают, что при больших скоростях вращения течение является трехмерным и заметно его влияние на теплообмен. Измерены средние числа Нуссельта. Для двумерных моделей при значениях σ, больших единицы, вычислены характеристики теплообмена.